Novel reference standards for the qualification of radiography-based computed tomography simulation software

Fabrício Borges de Oliveira[1], Tamara Reuter[2], David Plotzki[3], Markus Bartscher[1], Tino Hausotte[2]

[1]Physikalisch-Technische Bundesanstalt (PTB), Bundesallee 100, 38116 Braunschweig, Germany, e-mail: fabricio.borges@ptb.de, markus.bartscher@ptb.de

[2]Institute of Manufacturing Metrology (FMT), Friedrich-Alexander-University Erlangen-Nuremberg (FAU), Nägelsbachstraße 25, 91052 Erlangen, Germany, e-mail: tamara.reuter@fmt.fau.de, tino.hausotte@fmt.fau.de

[3]Bundesanstalt für Materialforschung und -prüfung (BAM), Unter den Eichen 87, 12205 Berlin, Germany, e-mail: david.plotzki@bam.de

Abstract

This contribution presents a set of largely novel reference standards specially designed for testing different important physical effects and functionalities of radiography-based computed tomography (CT) simulation software. These standards were developed within the scope of the German cooperation project "CTSimU – Radiographic Computed Tomography Simulation for Measurement Uncertainty Evaluation" [1] and serve as tools for the *basic qualification* of the sufficient physical correctness and required features of simulation software of CT-based coordinate measurement systems (CMSs) via the analyses either of 2D projection images only or of full CT scans. The results serve as input to the German standardisation committee for the development of a new national VDI/VDE guideline in the series VDI/VDE 2630 dealing with the *basic qualification* aspect of CT simulation software and shall lay ground for the measurement uncertainty determination of dimensional measurements using CT.

Keywords: Radiographic simulation software, basic qualification, CT simulation, spherical step-wedge, conical hole sheet, Tungsten-Edge, Multi-geometry cuboid, WIPANO CTSimU Project

1 Introduction

The demand for more precise and reliable measurements with X-ray computed tomography (CT) is increasing with the growing importance of CT for coordinate metrology. Despite many enhancements achieved in the recent years, regarding hardware, software and normative developments, CT has not yet reached the same level of confidence as tactile and optical coordinate measurement technologies. This is mainly because the traceability of CT measurements to the metre could not be yet stablished, especially because of the complex interaction of a large number of factors influencing the measurement results, which hinders (to a large extend) the task of measurement uncertainty determination.

Conventional methods of measurement uncertainty estimation used in coordinate metrology often require either a comprehensive understanding of the measurement process, including all relevant factors influencing the measurement (e.g., GUM-method [2]); or require a large effort by performing repeated measurements of a calibrated standard (as described for tactile systems in ISO 15530-3, VDI/VDE 2617-8 and specifically for CT in VDI/VDE 2630-2.1). The high complexity of CT measurements and the costs associated to the repeated measurements or the ability to simply calibrate a workpiece entirely limit the application of these methods to CT measurements.

Thus, the interest in simulations as a tool for determining the uncertainty of CT measurements, according to the method described in the GUM Supplement 1 [3], has been significantly growing among industry and research. Additionally, CT simulation software (simulators) potentially yield more information with less effort. So far, several software packages are available for the simulation of radiographies for CT measurements [4-10]. They have already been used in research and industry for various applications, e.g., [11-15]. However, an important obstacle to use simulation software for general dimensional metrology purposes, or even estimation of measurement uncertainty is the lack of standardised procedures (e.g., a guideline or standard) available on how to qualify a simulation software for these purposes. Before a CT simulator can be used for a task- and CT system-specific measurement uncertainty determination, it has to be ensured that the physical laws, characteristic effects and basic functionalities of the CT measurement process are correctly enough reproduced by the simulator. In other words, the software needs to be validated for specific tasks related to dimensional measurements. The *basic qualification* of a simulator is a first required step in such a validation process.

The German WIPANO funded research project "CTSimU – Radiographic Computed Tomography Simulation for Measurement Uncertainty Evaluation" [1] approaches, as the name suggests, the use of CT simulation for estimating the measurement uncertainty. Due to the complexity of the topic, the approach was divided into three sequential research projects: (1) the *basic qualification* of CT simulation software (finished WIPANO project [1]); (2) the construction and verification of digital twins (already granted – CTSimU2) and (3) the estimation of the measurement uncertainty (planned CTSimU3). The *basic*

https://doi.org/10.58286/26578

qualification as the first step consists of checking requirements for simulation software and performing a test framework to check the conformity of these requirements. The requirements list the basic physical effects and functionalities to be fulfilled by a CT simulator, demonstrating their capability to simulate relevant effects and functionalities for specific dimensional measurement tasks. The test framework is designed to systematically test whether a simulation software fulfils the requirements, based on a set of specific 2D and 3D tests. The 2D tests are carried out based on a single or a few 2D projections of specifically designed test scenarios to evaluate one or more physical effects or functionalities based on 2D imaging processing. Additionally, the 3D test considers the entire CT measurement chain. Therefore, the data evaluation is based on simulated 3D measurements of a specially designed 3D test scenario carried out on the reconstructed volume.
This contribution focuses on a set of novel reference standards used for the *basic qualification* of CT simulation softwares for the use in coordinate metrology. These standards were designed, for this virtual purpose only, i.e., to test analytically basic physical effects and functionalities of CT simulators. Designing the standards just for virtual use allows to design them to be as sensitive as possible to the tested effects, without considering manufacturability constraints. This *basic qualification* provides an important requirement to accomplish reliable uncertainty determination of dimensional CT measurements using simulation in future. Describing such a *basic qualification* represents a technological progress itself which can create trust in simulators. But for a broader use of such "tools" in industry and commerce, a consolidation of the achieved technical level is helpful or may be even required. Therefore, a further important outcome of the research project is a draft of a VDI/VDE guideline on the *basic qualification* of CT simulators. The activity in VDI/VDE on this topic has already started in Oct. 2021.

2 Reference standards for the qualification of radiography-based CT simulation software

Four mostly novel standards were designed to test the sufficient reproduction of physical effects and functionalities of CT simulation software relevant for coordinate metrology. Three of them, the *conical hole-sheet (HS)*, the *spherical step-wedge (SW)* and a *Tungsten-edge standard (WE)* are used to test effects based on a single or a few 2D projection images. The *multi-geometry cuboid* was designed as a complex 3D standard to test the simulation software based on complete CT scans. These standards will be presented in detail in the following sections.

2.1 Conical hole-sheet standard

The *conical hole-sheet* standard (*HS*) was designed to verify if a CT simulation software is able to correctly position and orient the main components of a CT system (i.e., X-ray source, object/rotary table and detector). The *HS* has a size of approximately 11.2 mm × 11.2 mm × 0.05 mm (Figure 1) and it features 10 hole-like structures with a distorted conical shape, which are oriented along the X-ray trajectories from the point of the X-ray source to individual points on the detector. Figure 1-c displays schematically the construction of the hole-like structures. For the sake of simplicity, these nearly hole-like structures will, from now on, simply be called "holes". With this oriented distortion, the individual holes are each projected onto the detector as perfect circles with optimally sharp edges (i.e., in a completely ideal simulation scenario), see Figure 1-c. The projected sharp edges significantly help the edge detection algorithm (in the data processing step) to determine the edges of the circle as precisely as possible and as a consequence also the centre position and diameter of the circle. Nine out of ten holes have the same projected diameter (20 mm), one of them, hole "0", has a larger projected diameter (40 mm) and it is also used to break the symmetry of the standard, see Figure 1-b. The position and orientation of the CT components are tested by measuring the relative distances and angles between the projected hole centres as well as the diameters and positions of the holes.

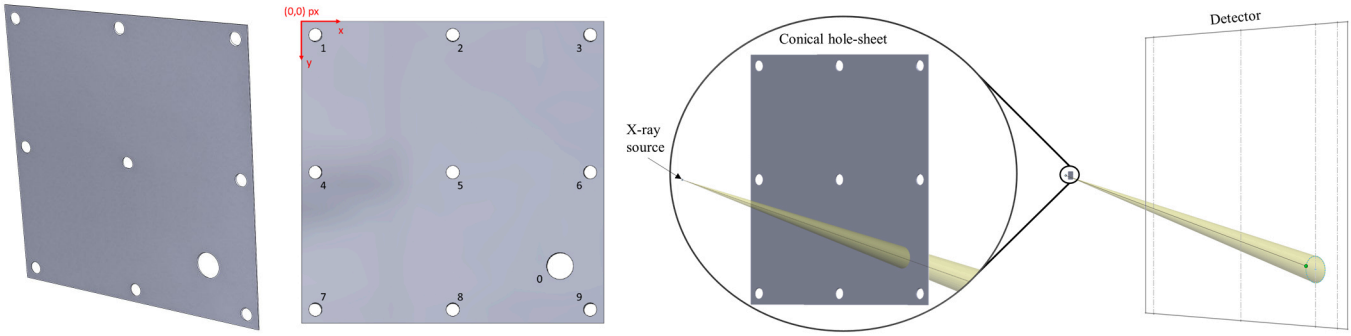

(a) (b) (c)

Figure 1. (a) Isometric view, and (b) front view of the conical hole sheet standard; and (c) illustration of how the distorted hole-like structures were constructed

Thanks to the flexibility of simulation, any material can be used in the simulations of the 2D imaging of the *conical hole-sheet* standard. However, in this study pure Tungsten was used, because of its very high attenuation coefficient providing sufficient contrast in the 2D images.

2.2 Concentrical spherical step-wedge standard

The *concentrical spherical step-wedge standard* (*SW*) was designed to verify several effects and/or functionalities of simulation software based on the grey value behaviour of a few 2D images. The following effects and functionalities can be tested with this design:

- detector's scintillator characteristic,
- spectral filter (metal plate placed at the exit of the X-ray source to attenuate low-energy photons),
- physical interaction between X-ray radiation and matter,
- calculation of the material penetration lengths,
- the behaviour of the simulators for object models featuring two neighbouring surfaces (i.e., touching surfaces and a small gap between) and overlapping object models,
- scattered radiation.

The design of the *step-wedge standard* (see Figure 2) consists of 9 spherical concentric steps, i.e., they were designed specifically to have the steps' common sphere centre for inner and outer surfaces lying on the focal spot of the X-ray source. An advantage of this design is that it allows a constant penetration length throughout the entire extension of each step. On the other hand, the constant material penetration length is only achieved if some requirements are met, e.g., if the standard is perfectly correct positioned in the simulation scene. If all requirements are met, a constant grey value profile over each step can be reached. Further mandatory testing conditions for the simulator are vacuum as the simulation environment, an infinitely thin detector with constant and equal sensitivity for each energy and an isotropic radiation of the X-ray source. The *SW* features steps with different thicknesses to cover a broad range of grey values being tested. The step thicknesses were designed to reach with the thinnest und thickest steps an X-ray transmission of 95% and 5%, respectively, at a defined polychromatic X-ray spectrum (e.g., *SW* made of Al and Fe were designed at $U_{Max,Al}$ = 120 kV and $U_{Max,Fe}$ = 200 kV and no filter, respectively). The thickness of the middle steps (steps 2 - 8, Figure 2-c) change linearly between the two extremes (step 1 and 9). The height and width of the *step-wedge* was designed based on the projected square-shaped image onto the detector for the CT setup specified for this test. In the projected image, the height of each step appears to be the same, and it covers 1/11 of the detector's vertical extension. Regarding their width, a single step covers also 9/11 of the detector's horizontal extension. The reason to leave part of the detector freely exposed at each boundary is that the free beam areas are also used in the test evaluations. The transition regions between steps were designed (similar to the holes in section 2.1) to follow the X-ray path from the source to the detector, guaranteeing sharp transition edges and a maximum usage of the projected step areas. A chamfer was included at the right corner of the thickest step to break the symmetry of the standard, see Figure 2 (a) and 2 (c).

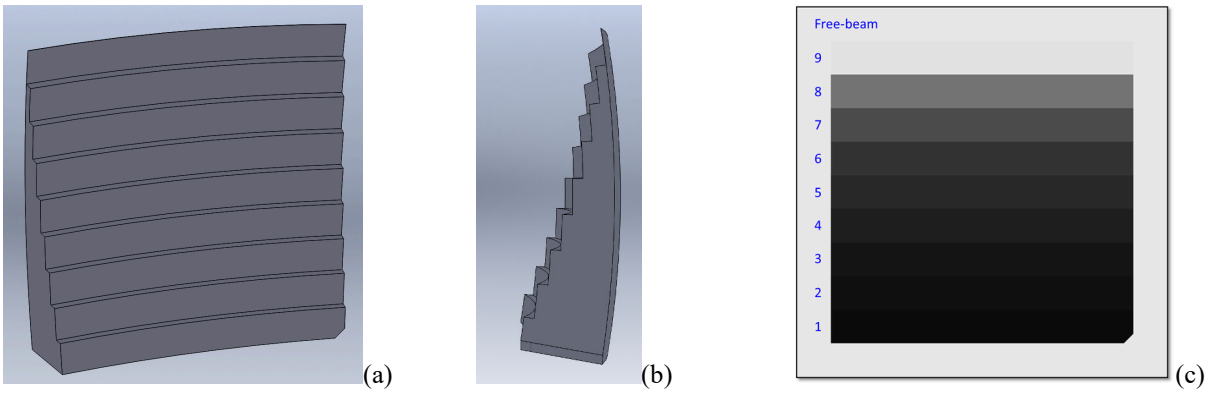

(a) (b) (c)

Figure 2. (a) *Spherical concentric step-wedge standard*; (b) side view of the *step-wedge standard*; and (c) projection image created with the *step-wedge*; observe also the steps numbers, the free-beam area around the projected image and the chamfer on bottom right of the standard.

Figure 3 schematically shows the construction of the *step-wedge standard*, where the material "cut" (illustrated by the two yellow triangles) was based on the X-ray path from the X-ray source to a specific position on the detector.

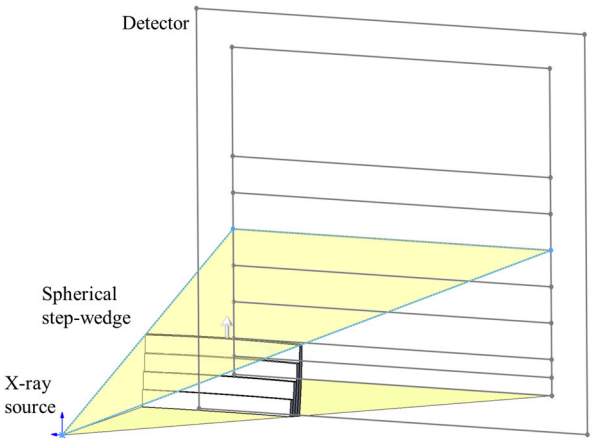

Figure 3. Illustration of the construction of *spherical step-wedge standard*, where the material "cut" (illustrated by the two yellow triangles) was based on the X-ray path from the X-ray source to a specific position of the detector.

To enable the test based on grey values with two different materials, two designs (small and large) of the *step-wedge* with the same design requirements were created. The materials selected are Al and Fe, covering a rather large attenuation coefficient range as well as representing materials commonly used in industry and coordinate metrology. The designed curvature radii and thicknesses of both designs of each spherical step are listed in Table 1.

Table 1. Radii and thickness of each step of both (a) large – Al and (b) small – Fe designs of the spherical concentric *step-wedge*. All units are given in mm.

Large (Al)	R1	R2	Thickness
Step 1	477.02	518.02	41.00
Step 2	482.13		35.89
Step 3	487.23		30.79
Step 4	492.34		25.68
Step 5	497.45		20.58
Step 6	502.55		15.47
Step 7	507.66		10.36
Step 8	512.77		5.26
Step 9	517.87		0.15

(a)

Small (Fe)	R1	R2	Thickness
Step 1	244.39	254.39	10.00
Step 2	245.63		8.76
Step 3	246.88		7.51
Step 4	248.13		6.26
Step 5	249.38		5.01
Step 6	250.62		3.77
Step 7	251.87		2.52
Step 8	253.12		1.27
Step 9	254.37		0.02

(b)

For testing scattered radiation, neighbouring surfaces, and overlapping virtual object models, the design of the *spherical step-wedge* was modified. (1) For the scattered radiation test, the original standard design was "cut" in half vertically, i.e., the half *spherical step-wedge standard* still contains all 9 steps, however with half of their original width. This design allows the evaluation of scatter radiation in free beam regions close and far from different material penetration lengths. (2) For testing the simulation's behaviour at neighbouring surfaces (i.e., directly in contact or with a small gap between them) as well as partially overlapping object models, two "almost" half *spherical step-wedges* were created. One half of the object model has a straight cut in its half (same design used in the scattered radiation test (1)). The other half was designed featuring three adapted regions (each region covers of the vertical extension of 3 steps) with different characteristics. The region at the top has a slight tilted surface (by an angle of 1.0503°) creating a decreasing (from top to bottom) gap between the surfaces. In the designed simulation scene, this small tilt angle was selected to reach an open gap with a maximum width of 5 pixels at the top, considering that at the lowest point of the region both halves are precisely in contact. In the middle region of the standard, both halves are perfectly in contact, where the half with tilted surfaces of the design features also a straight "cut". The lower region also features a tilted surface (by an angle of 2.0999° reaching a maximum overlap of 10 pixels), however, this time towards the other half to achieve an overlapping region of both halves, see Figure 4.

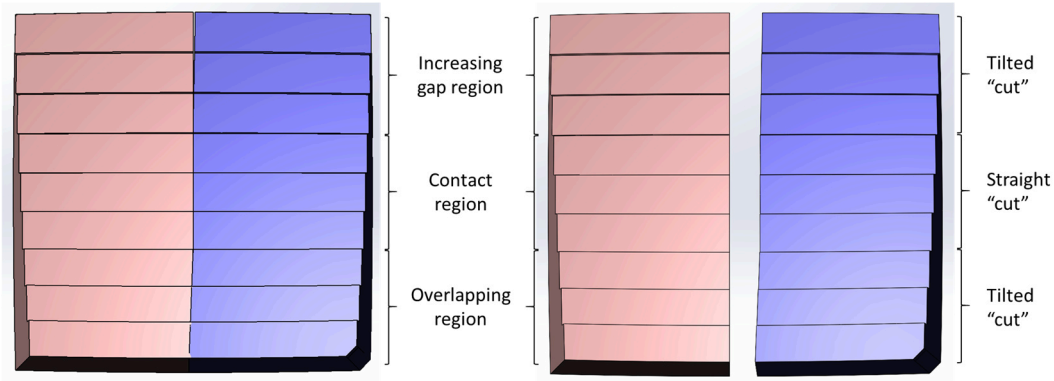

Figure 4. Modified design of the spherical concentric *step-wedge standard*, which consists of two almost half *step-wedges* for testing scattered radiation, neighbouring surfaces and models with overlapping regions. (Left) “Mounted” stated of the two halves. (Right) The two halves are shown separated (only to allow for a view of the structures hidden in left part of this Figure).

2.3 Inclined Tungsten edge standard

The *inclined Tungsten Edge standard* (*WE*) was designed to test the behaviour of the simulation software for detector pixels that are partially covered by a high absorbing material; and if the simulator can correctly reproduce spatially extended focal spots. For the first aspect, the grey value behaviour of the partially covered pixels is analysed and compared with the analytically calculated image. For the latter aspect, the 2D extension of the focal spot can be analysed based on the modulation transfer function (MTF) of a profile perpendicular to the object edge. The standard consists of a 4 mm thick block, with 3° inclined edges to minimise aliasing effects and to reach different coverage of different pixels, see Figure 5. Besides that, to guarantee equal penetration lengths for all X-ray paths travelling through the *Tungsten edge*, as a newly introduced feature, the relevant edges (i.e., two edges to be measured) were constructed following the X-ray path from the source to the detector (i.e., mathematically described as ruled surfaces). The profiles perpendicular to the object edge are measured in two the non-planar ruled surface side faces, see Figure 5. This helps to achieve maximum edge sharpness in the projected image. In the test simulations carried out for this work, pure Tungsten was used as material, to reach (in good approximation) full absorption of the photons being emitted from the source to the detector in the edge region.

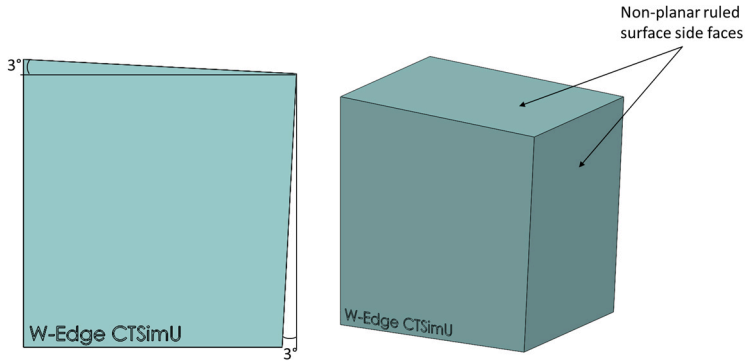

Figure 5. *Inclined Tungsten edge* standard featuring two parallel planar front and back faces and two non-planar ruled surface side faces.

2.4 Multi-geometry cuboid

The novel *multi-geometry cuboid* (see Figure 6) is designed as a prismatic reference standard to qualify CT simulators to perform a correct complete CT scan based on selected dimensional evaluations of a complex technical part (3D test), including all steps of the measurement chain (i.e., CT scan, reconstruction, surface determination and dimensional analysis). Although the task of the simulation software is limited to the first step of the measurement chain (i.e., creating the projection images only), this design is used to verify that an entire CT scan is correctly carried out by the simulator (i.e., if all projections are taken correctly and to test effects separately). The subsequent data analyses are based on dimensional measurements on the reconstructed volume. The *multi-geometry cuboid* has a designed size of 22.2 mm × 21.8 mm × 15.0 mm and features 37 inner and outer geometrical elements (i.e., cylinders, cones, planes, half-spheres/calottes, tori), see Figure 6. From these geometries, 68 measurands of different complexity (including e.g., distances, diameter, cylindricity, concentricity, etc.) are derived and proposed in this contribution. To facilitate the data evaluation, the designed measurands are categorised into classes: size (angle, diameter, radius, distance), form (flatness, circularity, roundness, cylindricity), position (concentricity, coaxiality) and orientation (parallelism, perpendicularity) measurements. The selection of the measurands was motivated to cover a large range measurands typical for industrial use. The set of measurands include intentionally both simple and relatively complex measurement tasks and shall in total also guarantee that potential undesired effects and hidden errors in the simulators are detected. A previous version of this

reference standard design was already presented and tested [16]. The current version of the standard is also being used to test geometrical detector misalignments in a parallel contribution to iCT 2022 [17].

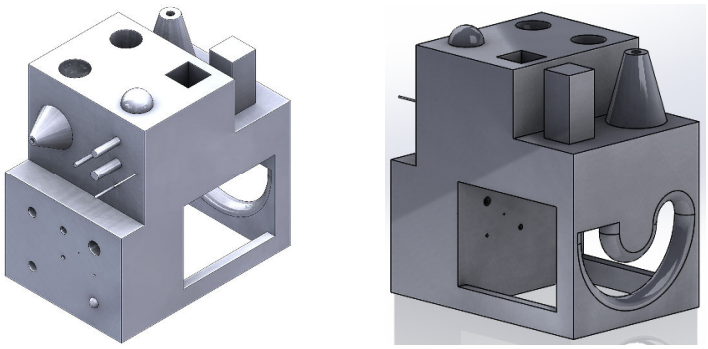

Figure 6. Front and back view of the novel *multi-geometry cuboid*.

The geometrical elements of the standard are named according to their type and position on the standard's surface. The naming of all elements is presented in Figure 7. (Notation: Plane: *Pla*, Sphere: *Sph*, Calottes: *Cal*, Cuboid: *Cub*; Cylinder: *Cyl*, Cone: *Con*, Tori: *Tor*).
Additionally, an overview of all 68 measurands being measured with their respective geometrical element in the multi-geometry cuboid is presented in Table 2. The measurands presented here are all based on the total least-square fitting of the geometrical elements without a constraint of size and position of the elements.

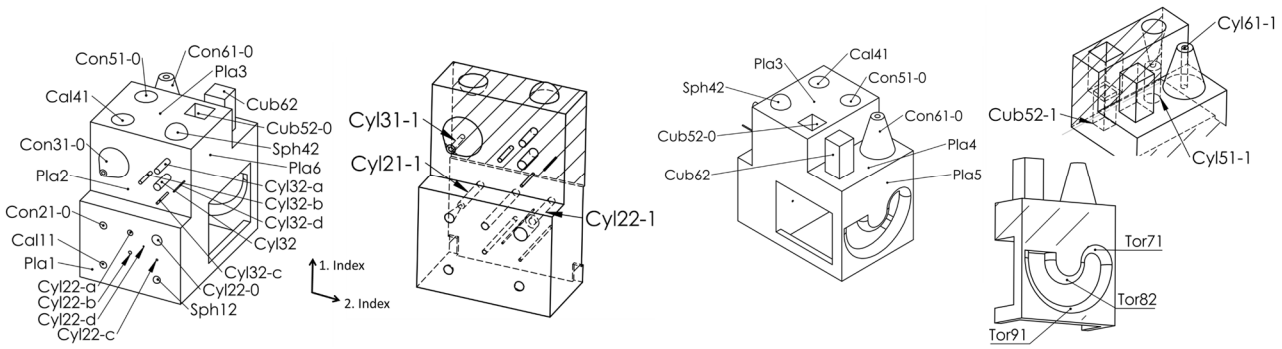

Figure 7. Label of all measured geometrical elements of the multi-geometry cuboid.

Table 2. Overview of the measurands with their respective geometrical elements (reference elements are highlighted in bold and underlined)

Measurand type	**Name**	**Geometrical elements used**				
Diameter	Dia	Cal11	Sph12	Cal41	Sph42	Cyl22-0
		Cyl22-a	Cyl22-b	Cyl22-c	Cyl22-d	Cyl32
		Cyl32-a	Cyl32-b	Cyl32-c	Cyl32-d	Cyl51-1
		Cyl61-1a	Cyl61-1b	Cyl61-1		
Torus major radius	MajRad	Tor71	Tor81	Tor91		
Torus Minor radius	MinRad	Tor71	Tor81	Tor91		
Cone opening angle	Ang	Con21-0	Con31-0	Con51-0	Con61-0	
Centre-to-centre distance	Dis	Cal11--Sph12		Cal11--Cal41		Cal11--Sph42
Point-to-point distance	Dis	Poi52-0b--Poi62-0b		Poi52-0b--Poi62-0d		Poi52-1c--Poi51-1c
		Poi52-1c--Poi51-1a				
Perpendicularity	Per	Cub52-0b--**Cub52-0c**		Con21-0--**Cyl61-1**		Cyl31-1--**Con51-0**
Parallelism	Par	Cub62-c--**Cub62-a**		Cyl51-1--**Con61-0**		Cyl32--**Con31-0**
Coaxiality	Coa	Con21-0--**Cyl21-1**		Cyl31-1--**Con31-0**		Con51-0--**Cyl51-1**
Concentricity	Con	Cyl61-1a--**Con61-0**		Cyl61-1b--**Con61-0**		Cyl61-1c--**Con61-0**
Sphericity	SFo	Cal11	Sph12	Cal41	Sph42	
Cylindricity	Cyl	Cyl22-0	Cyl22-a	Cyl22-b	Cyl22-c	Cyl22-d
		Cyl32	Cyl32-a	Cyl32-b	Cyl32-c	Cyl32-d
		Cyl51-1				
Roundness	Rou	Cyl61-1a	Cyl61-1b	Cyl61-1c		
Flatness	Fla	Cub52-0a	Cub52-1d	Cub62-b		

3 Systematic applications of the new reference standards

This section is dedicated to present first applications of the developed reference standards and aims to demonstrate that the standards and the evaluation methods are sensitive even for small deviations from the ideal / analytical physical effects or functionalities being tested. The simulations were carried out using ideal simulation conditions (except for the intentionally induced deviations) in the simulation software aRTist 2.10 (BAM, Berlin). For all presented results of the 2D tests, the Analysis Toolbox [18,19] developed in the CTSimU project was used to carry out the data analyses.

3.1 Application of the *conical hole-sheet standard*

For the systematic application of the *conical hole-sheet*, the standard was intentionally false positioned and also false oriented in the simulation scene to demonstrate that the standard and the data evaluation procedure, based on a few 2D images, are able to detect even small geometrical deviations of the system geometry. For that, three projections were simulated: one featuring an ideal system geometry (no false position; no false orientation), where the relative distances between source, rotary table and detector were set up according to the original design of the *conical hole-sheet*; a simulation featuring intentionally induced geometric deviations; and a respective free-beam image for the flat-field correction. In this example, the rotary table axis was positioned -4.6 µm in x direction deviating from the designed position. The rotary table axis was tilted by 0.15° and -0.14° around $\vec{u}$ and $\vec{v}$, respectively. (see Figure 8 for axis designations) These deviations represent realistic values for small system geometry error to be observed for industrial CT systems. The X-ray source, rotary table / object and detector were arranged to reach a magnification of approximately 40.

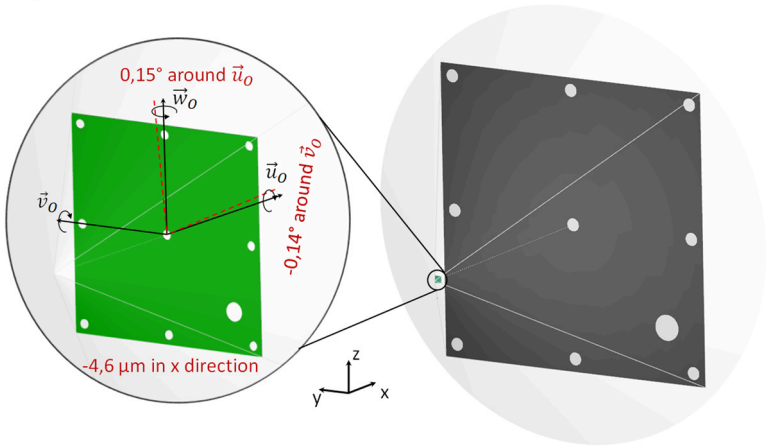

Figure 8: Scheme of the simulation scene, including geometrical deviation, used to verify the *conical hole-sheet* standard.

The evaluation of the 2D scenario is based on the measurement of the scale error, where the distances between each hole pair are measured; the *hole-sheet* rotation by means of measuring the relative angle between hole pairs as well as translation measured based on the position of the hole centre coordinates. More information on data evaluation can be found in [19]. Table 3 displays the results of the deviated and ideal system geometry for all measured quantities.

Table 3: Results of the example of a systematic application with the *hole-sheet* standard, where the geometry of the virtual CT system was intentionally false positioned. The standard deviation refers to the root mean square error (RMSE) for all measured hole pair combinations.

	Scale error		Rotation in °		Mean translation in px		Standard deviation of mean translation in px	
	Mean	**Standard deviation**	**Mean**	**Standard deviation**	**in x-direction**	**in y-direction**	**in x-direction**	**in y-direction**
Ideal geometry	$2.40\ 10^{-6}$	$1.33\ 10^{-5}$	$-2.88\ 10^{-5}$	$9.06\ 10^{-4}$	$1.01\ 10^{-3}$	$-1.93\ 10^{-3}$	$1.59\ 10^{-2}$	$1.60\ 10^{-2}$
Deviated	$3.49\ 10^{-4}$	$9.46\ 10^{-4}$	$1.49\ 10^{-1}$	$3.48\ 10^{-2}$	$-5.36\ 10^{-1}$	-1.68	1.16	$8.23\ 10^{-1}$

The misplacement of the rotary table can be mainly observed by the increase of the mean scale error ($-2.40.10^{-6} \rightarrow 3.49.10^{-4}$, cf. Table 3). The rotation around $\vec{u}_o$ is mainly detected by the increase of the *hole-sheet* mean rotation ($-2.88.10^{-5} \rightarrow 1.49.10^{-1}$, cf. Table 3). The misalignment around $\vec{v}_o$ is primarily detected by the increase of the standard deviation of the scale error and of the translation — caused by a trapezoidal distortion — (scale error $1.33.10^{-5} \rightarrow 9.46.10^{-4}$ and translation in x direction: $-1.93.10^{-3} \rightarrow 1.68$ and in y direction: $1.60.10^{-2} \rightarrow 8.23.10^{-1}$, cf. Table 3). The results indicate that the *hole-sheet* and the evaluation method were able to detect even small geometric deviations, presenting a significant difference between the deviated and ideal geometry. The authors are aware that for a better interpretation of the results, a conformity interval (i.e., range of results which are considered acceptable for the tested effect) is necessary, this point will be addressed in a future publication.

3.2 Application of the *spherical step-wedge standard*

The selected setup to demonstrate the use of the *spherical step-wedge standard* is based on two object models nearby placed in the simulation. The analysis toolbox verifies the presence of pixel anomalies based on a few 2D X-ray images. In this example, the modified design consisting of two *step-wedge* "halves" was used (see Figure 4). Aluminium and Titanium were assigned to the straight half and the half with tilted surfaces, respectively. In this example the Titanium half should be selected as dominant material over aluminium, i.e., in the overlapping region the aluminium material shall not be considered by the simulation software. Additionally, an anomaly was intentionally added in the overlapping region of the second thickest step of the step-wedge, where a (vacuum) cavity in an elliptic cylinder shape was included in the overlapping bottom region from the straight to the tilted halves in step 2, see Figure 9-a. This example aimed to demonstrate the suitability of the design for this test and that the data analysis applied in this test is sensitive even to small anomalies of the object model.
The data evaluation is based on the expected grey value behaviour, i.e., change of the grey values in the transition regions, in the correct position of the projected image. Therefore, it is required by the test that both halves to be correctly positioned in the scene. The expected grey values are calculated based on the exponential attenuation law, depending on the X-ray energy and the materials in use. More information on the data evaluation can be found in [19].
The simulated grey values are compared with the analytical image. The presentation of the results is based on the number of pixel anomalies (i.e., the number of pixels showing a relevant deviation from the expected grey value) found in the simulated image. Additionally, an image grey map (Figure 9-b) displays where these anomalies were found. In the image grey map the toolbox calculates the gradient in x direction of difference between the simulated and analytical images.
In the example tested in this contribution 83 pixel showing deviations / anomalies were detected in the region where the elliptic cylinder was inserted, see Figure 9-b. These pixel anomalies resulted in mean grey value of the anormal pixels of 1919.2.

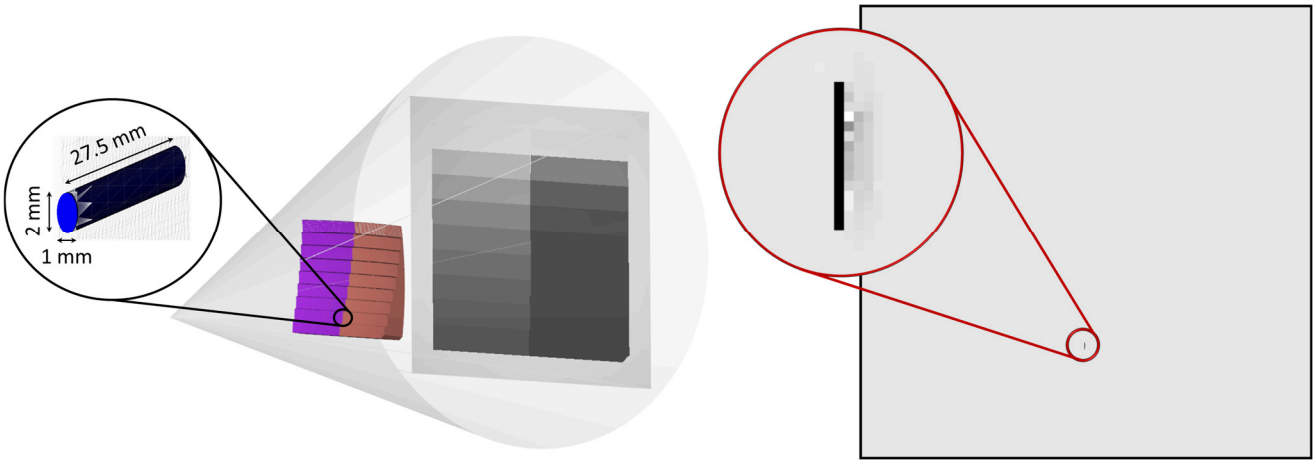

Figure 9. (a) Virtual scene for the simulation of the application of the modified design of the *spherical step-wedge standard*, where an anomaly (vacuum cavity in an elliptic cylinder form - in detail) was introduced to be detected; (b) resulting x gradient image grey map calculated based on the measured and analytical images. In this example, the image grey map displays the region of the step No. 2 (see Figure 2c.) where the effect of the anomaly is detected (see magnified insert).

3.3 Application of the *inclined Tungsten edge standard*

The example selected to demonstrate the use of the *inclined Tungsten edge standard* is based on the effect of partially covered detector pixels. For that, the specific parameter, i.e. the detector sampling, in the simulator aRTist was varied (set 1×1 and 5×5 as reference). In this simulation tool, this setting means that each detector pixel is being sub-divided into for instance 25 sub-pixel units for the "5×5 configuration" for the calculation of the final image (Figure 10), where for all sub-pixel units one ray will be traced from the source to centre of the pixel sub-unit centre. "The 1×1 configuration" means that the single pixel is considered as a single unit with exactly one ray being traced from the point source to its centre. This 1×1 behaviour leads to an incorrect representation of the partial coverage of a pixel and leads to only two possible grey values for any pixel (i.e., full coverage or full exposure), while the more correct behaviour would be to consider the fraction of the pixel area that is exposed to the beam and assign a grey value corresponding to this remaining intensity. The scheme of the used setup highlighting the partial coverage of some detector pixels as well as an illustration of a 5×5 detector sampling configuration in aRTist is presented in Figure 1Figure 10. For the simulations, an ideal detector was modelled, i.e., the detector was assumed to be infinitely thin; and the incoming radiation intensity is linearly converted into grey values without losses.
The data evaluation is based on the theoretical intensity at each pixel which is assumed to have 100% efficiency. The intensity is proportional to the incoming radiation flux, which in turn is proportional to the solid angle of the pixel's free (exposed) area as seen from the isotropically radiating source. An analytical image of the *Tungsten edge* is calculated, which allows a classification of all pixels. They can be either classified as completely or partially irradiated or completely covered. For the

partially irradiated pixels, the evaluation toolbox calculates the respective fraction of each pixel which is covered by the absorber. The test results are based on the number of partially covered pixels in the analytical and simulated images. These results are then compared to each other and the ratio (partly covered in both (analytical und simulated) / partially covered in the analytical) is also provided. The total root-mean-square-deviation (RMSD) between the grey values of the partially covered pixels found in the analytical and simulated images is also reported. Additionally, to better understand the practical meaning of the calculated RMSD value, the RMSD was divided by the edge length in pixel, where it was measured, see Table 4. The difference of about 20% of the number of partly covered pixels between the analytical and measured 5×5 images is explained by the detector sampling effect. For the 5×5 detector, pixels, which are exposed less than 1/25 or are covered more than 24/25 of their area are considered fully exposed or covered, respectively. For the 1×1 detector configuration, the software only considers completely covered or exposed pixels. More information about the data evaluation can be found in [19].

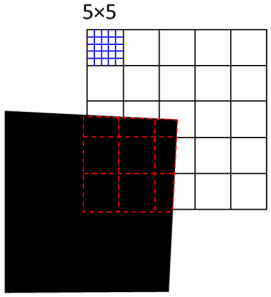

Figure 10. Illustration of the partially covered detector pixels by the *Tungsten edge*. In detail, in the top left an illustration of a 5×5 detector pixel configuration in aRTist, BAM, Berlin, is shown.

Table 4. Results of the 5×5 and 1×1 detector sampling tests using the *Tungsten edge* standard.

Metric	5×5	1×1
Number of partly covered pixels in analytical image	1053	1053
Number of partly covered pixels in measured image	844	0
Number of pixels partly covered in both images	844	0
Ratio (partly covered in both) / (partly covered in analytical)	80.1%	0.0%
RMSD [partly covered analytical vs. measured] in GV	4388.1	17312.5
RMSD / edge length (length in px) in GV/px	4.3	17.3

3.4 Application of the *multi-geometry cuboid*

In the application presented here, the *multi-geometry cuboid* is used to test whether the effects of the detector sampling are "visible" in 3D measurements in the CT reconstructed volume. For this purpose, the detector sampling configuration in aRTist was set to 1×1 and 5×5, comparable to the 2D example described in section 3.3. A source-object (SOD) and source-detector (SDD) distance of 127.5 mm and 2125 mm was used, respectively. An ideal energy-integrating detector was modelled, i.e., the detector was assumed to be infinitely thin; and the incoming radiation intensity is linearly converted into grey values without losses. The detector has 1000 px × 1000 px with a pixel size of 0.680 mm × 0.680 mm, leading to a voxel size of 40.8 µm. The point source emits a polychromatic X-ray spectrum with a tube acceleration voltage of 150 kV and a 4 mm aluminium filter. The tube's power, the integration time and the detector response were arranged in such a way that the grey values reach a maximum of 60000 at the free beam. To better evaluate the effect of detector sampling in the 3D measurements, further possible quality degrading effects (e.g., noise, detector unsharpness, spot size) were turned off for these simulations.
The flat-field correction of the projection images was carried out using the CTSimU Toolbox [18]. The reconstruction of the 2D and the 3D data evaluation were carried out using the commercial evaluation software VGStudio Max 3.4.5 (Volume Graphics, Heidelberg) and it is based on the 68 measurands proposed for the multi-geometry cuboid described in section 2.4. The surface from the volumetric data was determined by a local adaptive algorithm implemented in VG Studio Max using standard settings.

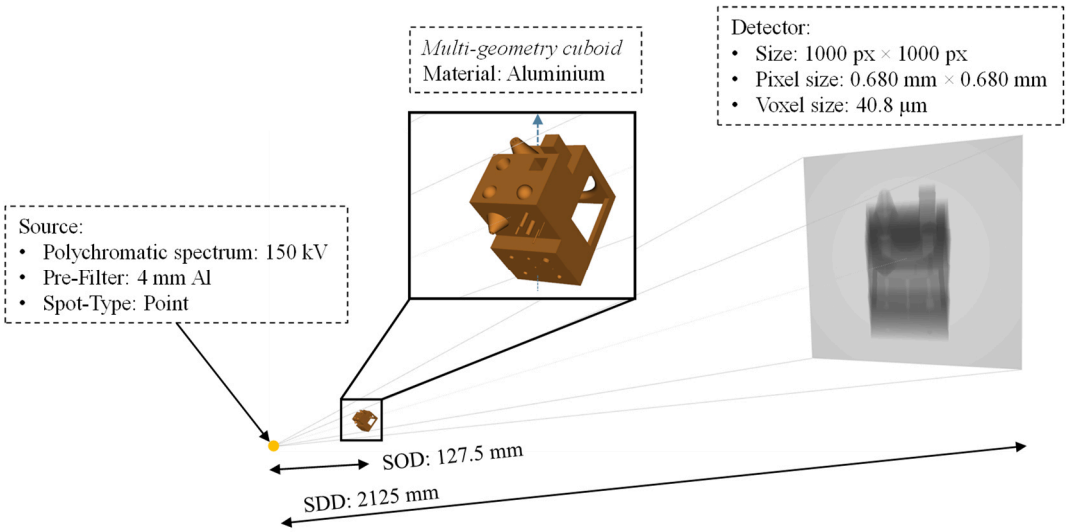

Figure 11. Scheme of the setup used for testing the detector sampling configuration of aRTist based on 3D measurements using the *multi-geometry cuboid* (Source: Figure adapted from [17]).

The results of the 3D evaluations on the 68 measurands of the *multi-geometry cuboid* for the two detector sampling configurations under study (1×1 and 5×5) are presented in Figure 12. The plots show the difference between the respective dimensional analyses of the simulated data and the STL model used for the simulation. From the results, a strong increase in the deviation of the measurement deviations (i.e., higher difference between the simulated and STL data) for several measurands can be observed for the 1×1 detector sampling. This indicates a significant influence of the detector's setting regarding sampling, when measuring with a detector setting of 1×1 compared with the here assumed reference 5×5 setting as well as that the object design is suitable for detecting simulation errors related to detector sampling. From the results, it can be also seen that several measurands, even of a different category (e.g., size, form and orientation measurands) reacted sensitive to the effect under test.

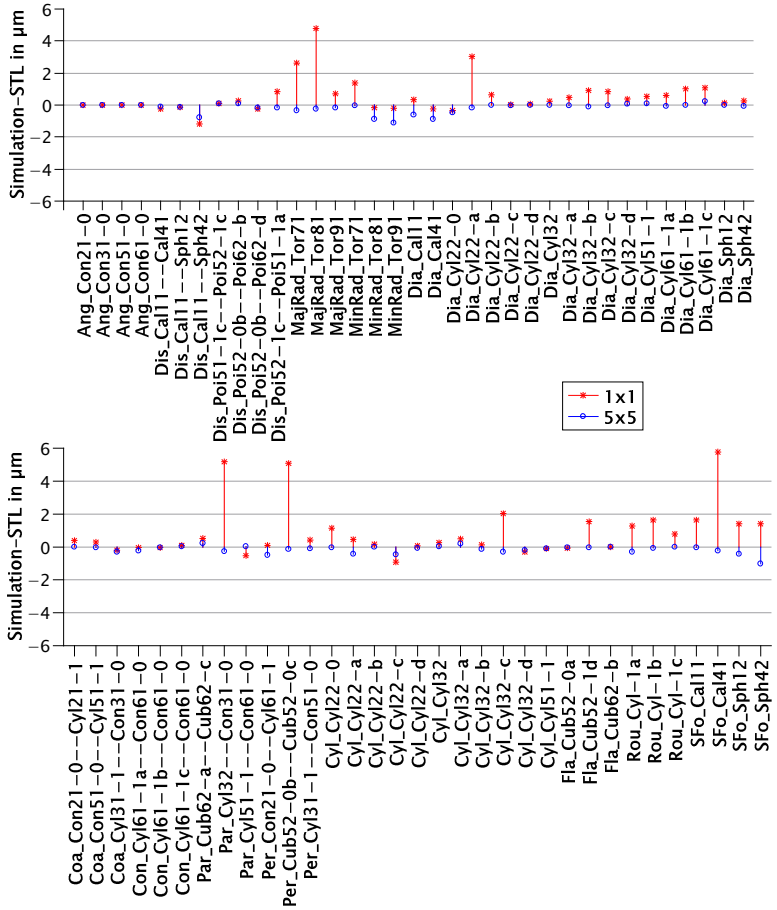

Figure 12. Results of all 68 measurands measured in the *multi-geometry cuboid* for testing the influence of the detector sampling effect on 3D measurements.

6 Summary and Outlook

A set of largely novel virtual reference objects for the *basic qualification* of CT simulation softwares was presented and described in this contribution: the *conical hole-sheet*, the *spherical step-wedge*, the *Tungsten-edge standards* and the *Multi-geometry* cuboid. These objects were designed to systematically test CT simulation softwares regarding specific physical effects and functionalities important to coordinate metrology tasks. The *conical hole-sheet* features 10 holes, which have a distorted conical shape and are oriented in the direction of the focal spot of the X-ray source. A similar approach was also applied in the *Tungsten-edge*, where its edges are ruled surfaces where the local tilt follows the incidence angle of the X-rays. The *spherical step-wedge* features 9 spherical steps, all of which are concentric and, thus, have a common centre in the focal spot, however each step has a different, but constant thickness for measuring different penetration lengths. These three standards were designed for evaluations of single projection images (2D tests) rather than complete CT scan simulations.
Additionally, the novel *multi-geometry cuboid* was presented. This prismatic reference standard is primarily used to test if a CT simulator is able to perform a complete CT scan based on a selected set of complex dimensional evaluations as a 3D test. The *multi-geometry cuboid* features 12 different kinds of geometrical elements (e.g. inner and outer cylinders, cones, planes, half-spheres, tori). A total of 68 measurands of different complexity (including e.g. size, form and position measurements) using this standard are selected. The data analysis is based on dimensional measurements of these 68 measurands on the reconstructed volume. An overview of the developed standards and examples of physical effects and functionalities that can be tested with each one of them is presented in Table 5.
In addition to that, a systematic application of the 2D and 3D standards was carried out. The application aims to provide an experimental feasibility test of the developed standards and analysis tools and shall also indicate if the developed standards and methods are potentially sensitive enough to detect even small errors of the simulation softwares under study. The results confirmed the sensitivity of the standards towards the tested effects, indicating the suitability of the standards to be used to qualify simulation software for metrological tasks. However, a more thorough sensitivity test of the standards considering further relevant effects still needs to be carried out. Examples of such tests were published and can be seen in [16] and [17].

Table 5. Overview of the designed reference standards with examples of effects and functionalities tested.

	Standard	Tested effect or / and functionality
2D	*Conical hole-sheet* (*HS*)	Relative position of the CT's main components (i.e. X-ray source, rotary-stage and detector)
2D	*Spherical step-wedge* (*SW*)	Grey value behaviour based on e.g. object material, X-ray penetration length, scattering, overlapping objects, air gaps between objects
2D	*Inclined Tungsten edge* (*WE*)	Focal spot size, partially covered pixels (detector sampling)
3D	*Multi-geometry cuboid*	Complete CT measurement process: influence of physical effects based on 3D measurements; exclusion of hidden effects which are not covered by 2D standards testing

Acknowledgements

This work was performed within the scope of the WIPANO Project CTSimU (03TNH026D). The WIPANO funding Program is financed by the German Federal Ministry of Economic Affairs and Energy (BMWi) and managed by Project Management Jülich. The authors thank all CTSimU project partners for the valuable discussions and support.

Gefördert durch:
Bundesministerium für Wirtschaft und Energie
aufgrund eines Beschlusses des Deutschen Bundestages

References

[1] WIPANO CTSimU, https://www.ctsimu.forschung.fau.de/, 2021 (accessed 17 December 2021)
[2] BIPM, Evaluation of Measurement Data–Guide to the expression of uncertainty in measurement, 1995
[3] Joint Committee for Guides in Metrology (JCGM/WG 1): JCGM 101:2008 - Evaluation of measurement data - Supplement 1 to the Guide to the expression of uncertainty in measurement - Propagation of distributions using a Monte Carlo method. 2008
[4] aRTist - Analytical RT Inspection Simulation Tool. – unter http://artist.bam.de, abgerufen am 18. November 2020
[5] Hiller, J.; Fuchs, T. O. J.; Kasperl, S.; Reindl, L. M.: Einfluss der Bildqualität röntgentomographischer Abbildungen auf Koordinatenmessungen: Grundlagen, Messungen und Simulationen. In: tm - Technisches Messen 78 (2011), August, Nr. 7-8, 334–347. – DOI 10.1524/teme.2011.0137
[6] Reiter, M.; Erler, M.; Kuhn, C.; Gusenbauer, C.; Kastner, J.: SimCT: a simulation tool for X-ray imaging. In: 6th Conference on Industrial Computed Tomography, Wels, Austria (iCT 2016), 2016
[7] van Aarle, W.; Palenstijn, W. J.; Beenhouwer, J. D.; Altantzis, T.; Bals, S.; Batenburg, K. J.; Sijbers, J.: The ASTRA Toolbox: A platform for advanced algorithm development in electron tomography. In: Ultramicroscopy 157 (2015), Oktober, S. 35–47. – DOI 10.1016/j.ultramic.2015.05.002
[8] CIVA, NDT Simulation software. – unter http://extende.com, abgerufen am 18. November 2020

[9] 3D Image Analysis and Simulation. 2013. – unter https://www.empa.ch/web/s499/rt1-3d-image-analysis-and-simulation, abgerufen am 18. November 2020
[10] The Leader in NDE Simulation Software. – unter https://www.ndetechnologies.com/, abgerufen am 18. November 2020
[11] Fuchs, P.; Kröger, T.; Garbe, C. S.: Self-supervised Learning for Pore Detection in CT-Scans of Cast Aluminum Parts. In: International Symposium on Digital Industrial Radiology and Computed Tomography, 2019
[12] Matern, D.: Analysis of Cone Beam Artefact Influences with Respect to Calibration of Metrology Qualified X-Ray Computed Tomography Systems. In: 9th Conference on Industrial Computed Tomography (iCT), 2019
[13] Joint Committee for Guides in Metrology (JCGM/WG 1): JCGM 101:2008 - Evaluation of measurement data - Supplement 1 to the Guide to the expression of uncertainty in measurement - Propagation of distributions using a Monte Carlo method. 2008
[14] Hiller, J.: Abschätzung von Unsicherheiten beim dimensionellen Messen mit industrieller Röntgen-Computertomographie durch Simulation, Universität Freiburg, Diss., 2011
[15] Bircher, B. A.; Meli, F.; Küng, A.; Thalmann, R.: CT geometry determination using individual radiographs of calibrated multi-sphere standards. In: 9th Conference on Industrial Computed Tomography, Padova, Italy, 2019
[16] Ferrucci, M.; Leach, R. K.; Giusca, C.; Carmignato, S.; Dewulf, W.: Towards geometrical calibration of x-ray computed tomography systemsa review. In: Measurement Science and Technology 26 (2015), August, Nr. 9, 092003. – DOI 10.1088/0957–0233/26/9/092003
[15] Ferrucci, M.: Systematic approach to geometrical calibration of X-ray computed tomography instruments, KU Leuven, Diss., 2018
[16] T. Reuter, D. Plotzki, F. Borges de Oliveira, T. Hausotte, Simulative Untersuchung des Einflusses von Bildrauschen auf dimensionelle Messungen mit industriellen Computertomografen, DGZfP-Jahrestagung 2021, May 2021, available at https://jahrestagung.dgzfp.de/portals/jt2021/bb176/inhalt/p8.pdf (accessed 19.07.2021).
[17] T. Reuter, F. Borges de Oliveira, D. Plotzki, T. Hausotte, Influence of detector misalignments on different geometrical and dimensional measurands using a dedicated test specimen, submitted to iCT2022, Wels.
[18] D. Plotzki, B. Hartlaub, F. Borges de Oliveira, T. Reuter, F. Wohlgemuth, T. Hausotte, The *CTSimU* software toolbox for CT-related image processing and quality assessment, submitted to iCT2022, Wels.
[19] CTSimU Software Toolbox, https://github.com/BAMresearch/ctsimu-toolbox, 2021 (accessed 17 December 2021)